Progress In Electromagnetics Research Letters, Vol. 28, 9–21, 2012

THREE-DIMENSIONAL FDTD ANALYSIS OF THE DUAL-BAND IMPLANTABLE ANTENNA FOR CONTINUOUS GLUCOSE MONITORING

Z. Noroozi* **and F. Hojjat-Kashani**

Department of Electrical Engineering, Iran University of Science and Technology, Tehran, Iran

Abstract—The finite difference time domain (FDTD) method is widely used as a computational tool to simulate the electromagnetic wave propagation in biological tissues. When expressed in terms of Debye parameters, dispersive biological tissues dielectric properties can be efficiently incorporated into FDTD codes. In this paper, FDTD formulation with nonuniform grid is presented to simulate a dual medical implant communications service (MICS) (402–405 MHz) and industrial, scientific, and medical (ISM) (2.4–2.48 GHz) band implantable antenna for continuous glucose-monitoring applications. In addition, we present computationally simpler two-pole Debye models that retain the high accuracy of the Cole-Cole Model for dry skin in MICS and ISM bands. The reflection coefficient simulation result with Debye dispersion is presented and compared with the published results. FDTD was also applied to analyze antenna's far-field.

1. INTRODUCTION

Recently, with the advances in telecommunications and telemedicine, implantable antennas are studied for several wireless applications such as artificial eyes, cochlear implants, brain and cardiac pacemakers [1–3], implantable drug pumps, hyperthermia treatment [4], etc. Scanlon et al. [5] performed numerical simulations for a printed loop antenna in a whole body phantom model (chest) at 418 MHz. Implantable antennas were the subject of a study reported by Kim and Rahmat-Samii [6]. In this study, they have designed a spiral microstrip and planar inverted-F antennas (PIFAs) at the MICS band based on the

Received 1 July 2011, Accepted 15 August 2011, Scheduled 29 November 2011

* Corresponding author: Zahra Noroozi (znoroozi@ee.iust.ac.ir).

FDTD simulations. They have also reported simulation results (based on FDTD) of the maximum available received power by an external (to the body) dipole antenna. Soontornpipit et al. [7], evaluated s_{11} of spiral and serpentine antennas at the MICS band. In a study by Warty and Tofighi [8], characterization of implantable PIFAs, designed for intracranial pressure (ICP) monitoring at 2.45 GHz, has been presented. In [9], an H-shaped cavity slot antenna was miniaturized and the characteristics of the antenna calculated by the FDTD method at the ISM band.

FDTD method, has become a popular numerical technique for analyzing the propagation of electromagnetic fields in the human body. For narrowband computations, the standard FDTD algorithm for lossy dielectric media can be used for biological tissues with acceptable accuracy. However, in broadband simulations by using a pulsed excitation, it is necessary to use time domain updating equations which incorporate the variation in the dielectric properties of tissues with frequency. Precise frequency dependent permittivity and conductivity values for biological tissues have been made available by Gabriel et al. that have been fitted by relatively complicated 4-pole Cole-Cole equations [10–12]. However, the implementation of the Cole-Cole model using the FDTD method is difficult because of the fractional order differentiators in this model. In some studies, least squares fitting technique has been applied to reduce Gabriel's 4-pole Cole-Cole equations to simpler 2-pole Debye equations [13–15]. In [16], a new FDTD formulation is presented for the modeling of electromagnetic wave propagation in dispersive biological tissues with the Cole-Cole model and the Z-transform is used to represent the frequency dependent dielectric properties.

This paper presents a two-step procedure for accurate simulation of a dual-band implantable antenna in dispersive media into the FDTD formulation. First, we present Debye parameters that describe the dispersive dielectric properties of dry skin tissue over considered frequency range (from 0.3 GHz to 3 GHz). The procedure employed here for fitting a Debye model to Cole-Cole data was previously described in [17]. Then FDTD formulation with nonuniform grid based on the Auxiliary Differential Equation Method (ADE) in conjuction with convolutional perfectly matched layered (CPML) is employed to simulate the dual-band implantable antenna for continuous glucose-monitoring applications [18] at the MICS and ISM bands. The resonance characteristics (in terms of s_{11}) of the dual-band antenna are computed and compared favorably with the published results in [18]. Also, the far-zone electromagnetic fields are computed from the near-field FDTD data through a near-field to far-field (NF–FF)

transformation technique [19].

2. TWO-POLE DEBYE DISPERSION MODEL OF HUMAN DRY SKIN

The general form of Cole-Cole formulation for the relative complex permittivity $\hat{\varepsilon}(\omega)$ is given in [12] as

$$\hat{\varepsilon}(\omega) = \varepsilon_\infty + \sum_n \frac{\Delta\varepsilon_n}{1 + (\mathrm{j}\omega\tau_n)^{(1-\alpha_n)}} + \frac{\sigma}{\mathrm{j}\omega\varepsilon_o} \tag{1}$$

where ε_∞ is the high frequency permittivity, τ_n is the relaxation time, $\Delta\varepsilon_n$ is the pole amplitude, α_n is the pole broadening and σ is the static ionic conductivity. The required general form of the Debye formulation is

$$\hat{\varepsilon}(\omega) = \varepsilon_\infty + \sum_{n=1}^{N} \frac{\Delta\varepsilon_n}{1 + \mathrm{j}\omega\tau_n} + \frac{\sigma}{\mathrm{j}\omega\varepsilon_o} \tag{2}$$

Using the "*residues*" Matlab procedure, the Debye coefficients (ε_s, τ_n, $\Delta\varepsilon_n$ and σ) were obtained and tabulated for 16 human tissues in the frequency range 0.75–250 MHz [20]. In this research, this procedure was applied to obtain complex permittivity of dry skin. The actual measurement data from [12] have been used instead of the Cole-Cole equation. The two-term Debye representation was sufficient to fit the data with an reliable error in the frequency range 0.3–3 GHz. The coefficients are given in Table 1.

In addition, we calculated the errors in the real and imaginary parts of the complex relative permittivity.

$$e_r(\omega) = \varepsilon'_d(\omega) - \varepsilon'_c(\omega) \tag{3}$$

$$e_i(\omega) = \varepsilon''_d(\omega) - \varepsilon''_c(\omega) \tag{4}$$

Table 1. Debye parameters for dry skin in the frequency range 0.3–3 GHz.

Debye parameters	Values for dry skin
ε_∞	4
$\Delta\varepsilon_1$	35.0558
$\Delta\varepsilon_2$	121.0454
τ_1 [s]	0.011×10^{-9}
τ_2 [s]	1.458×10^{-9}
σ [mS]	0.2

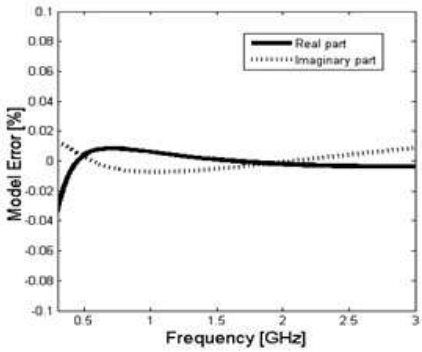

Figure 1. Error between the fitted measurement data [12] and a two-pole Debye model of dry skin with the parameters given in Table 1.

Figure 1 shows the errors in the real and imaginary parts of the relative permittivity as defined in (3) and (4) for the two-pole Debye model of dry skin from 0.3 to 3 GHz. For this model, the error is extremely small (0.02%).

3. A BRIEF REVIEW OF THE DUAL-BAND IMPLANTABLE ANTENNA

In [18], a dual-band implantable antenna intended for continuous glucose-monitoring applications was designed and *in vitro* tested. The top and side views of the initial antenna design are shown in Figs. 2(a) and (b), respectively. A serpentine configuration was considered for optimizing the antenna surface area and a shorting pin was used to assist in antenna miniaturization. This procedure typically produces the same frequency response at less than half the size of a similar antenna without the shorting pin [26]. Rogers RO3210 ($\varepsilon_r = 10.2$, $\tan\delta = 0.003$) was used for the substrate and superstrate material.

To tune and improve the antenna characteristics, at the MICS and ISM bands, particle swarm optimization (PSO) was applied. The length and width of the substrate were kept constant at $L_{sub} = W_{sub} = 22.5$ mm. The patch length and width also remained constant at $L_p = 22$ mm and $W_p = 17.75$ mm. Any remaining parameters were considered dimensions in the solution space.

For the optimization procedure, the antenna geometry was organized as shown in Fig. 3.

For improving antenna performance around the center frequencies of the MICS and ISM bands (402 MHz and 2.4 GHz), the fitness

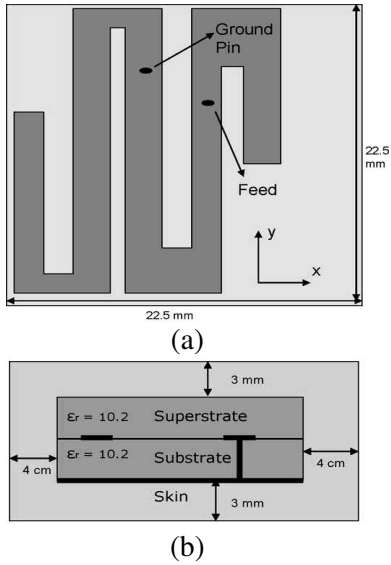

Figure 2. (a) Top and (b) side views of the initial antenna[18].

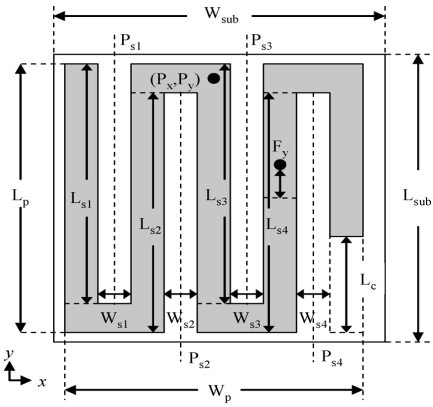

Figure 3. Optimization parameters [18].

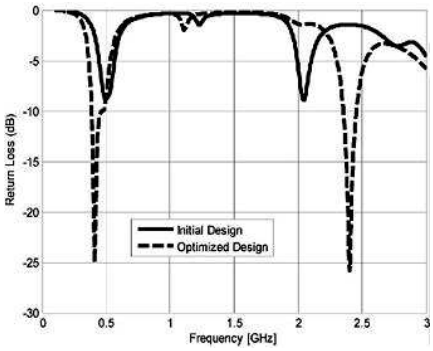

Figure 4. Return-loss comparison of the initial and optimized antenna designs [18].

function for PSO was defined as

$$\text{fitness} = \max\left(S_{11@402\,\text{MHz}}, S_{11@2.4\,\text{GHz}}\right) \tag{5}$$

and the objective was to minimize the fitness function. The optimized parameters are listed in Table 2 and Fig. 4 shows a comparison of the

Table 2. Optimization parameters.

Symbol	Optimized (mm)
P_{s1}	-7.0
W_{s1}	2.7
L_{s1}	19.1
P_{s2}	-3.9
W_{s2}	0.5
L_{s2}	20.1
P_{s3}	0.5
W_{s3}	2.0
L_{s3}	18.0
P_{s4}	3.5
W_{s4}	0.6
L_{s4}	17.5
L_c	9.6
F_y	0.1
P_x	0.2
P_y	0.2

optimized antenna to the initial design. The optimized antenna was fabricated and measured in a skin mimicking gel. The simulated and measured bandwidths were found to be 20.4% MICS, 4.2% ISM, and 35.3% MICS, and 7.1% ISM, respectively.

4. FDTD ANALYSIS OF DUAL-BAND IMPLANTABLE ANTENNA

4.1. Define Problem Space

The geometry of the FDTD simulations for the dual-band antenna is given in Fig. 5. For the ease of designing implanted antennas, three- and one-layer planar geometries, which provide an acceptable model for the human body, were proposed [6]. Based on the real human body structure, the three-layer geometry consists of skin, fat and muscle tissues and the one-layer geometry only includes a skin tissue. The metallic portion of the patch is assumed to be a perfect electric conductor with no thickness; It is sandwiched between substrate and superstrate dielectric layers whose permittivity is 10.2 and thicknesses

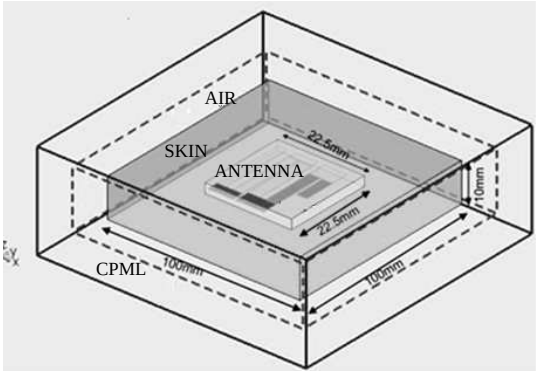

Figure 5. FDTD problem space.

are 1.25 mm. The whole antenna is positioned at the center in the horizontal xy-plane of the simplified body model, 4 mm under the skin. The body model is a rectangular box which corresponds to dry skin tissue characteristics at MICS and ISM bands and has dimensions of 100 mm, 100 mm, and 10 mm in the x, y, and z directions, respectively.

The geometrical details of antenna is small, leading to very small cell sizes. Further, to provide an acceptable model for the human body, antenna is located in a large dispersive medium. For uniform meshing, this two characteristics, produce very large lattice. A nonuniform grid, results in very small cells in the antenna region and coarser cells around [21]. In order to using the formulation of ADE technique described in [21], cell dimensions increase by one fifth in the dispersive medium. By changing the grid size very slowly, large local errors can be avoided. The standard FDTD notation for the dispersive medium based on ADE method can be found in [21]. The dimensions of the unit cell in the antenna region are $\Delta x = 0.14481$ mm, $\Delta y = 0.16294$ mm, and $\Delta z = 0.25$ mm. These cell dimensions increase by one fifth until reach to $\Delta x = \Delta y = 1.5$ mm, and $\Delta z = 1$ mm. The boundaries are terminated by a 10 cells thickness CPML and an air gap of 8 cells is left between the objects in the problem space and the CPML boundaries in the x and y directions and of 5 cells in the z direction. The overall lattice has a dimension of $223 \times 223 \times 64$ cells and a time step of $\Delta t = 0.289$ ps is used. The antenna is simulated by modeling of coaxial feeding line using a voltage source with 50 Ω internal resistor inside a feeding gap [22, 23]. The probe attaches to the microstrip patch at the top, while it stops one FDTD cell (0.25 mm) away from the ground plane at the other end. The excitation source is a gaussian pulse with a 3 dB cutoff frequency of 6 GHz that has enough energy

in the considered frequency range. Voltage and current are sampled across and around the voltage source, and they are tied together to form input port.

4.2. FDTD Subcell Modeling

Subcell modeling is often used in FDTD to model structures with dimensions much smaller than those of other elements in the overall grid. This method, resides on the idea of the contour path modeling technique which uses the integral form of Faraday's and Ampere's laws. To precisely model the antenna structure here, we have applied two subcell modeling techniques: the thin-sheet model (to model the zero thickness PEC objects include the radiator and the ground plane) and the thin wire model (to model the inner conductor of coaxial probe and the shortening pin).

In [19], a simple thin-sheet modeling technique with a reasonable accuracy for the majority of problems including zero thickness PEC strips, was discussed. In this method, any electric conductivity components surrounding and coinciding with PEC plates can be assigned the conductivity of PEC to model zero thickness PEC plates in FDTD method. The standard FDTD notation for the thin wire model can be found in [19, 24].

4.3. Radiation Pattern Computation

In FDTD method, the direct evalution of the far field calls for an excessively large computational domain, which is not practical in applications. Instead, the far-zone electromagnetic fields are computed from NF-FF transformation by integrating the tangential field on a Huygens' box [25]. In this work, far fields for all observation angles are required for 402 MHz and 2.4 GHz. For each frequency of interest a running Discrete Fourier Transform (DFT) of the tangential fields (surface currents) on a closed surface is updated at each time step. The complex frequency-domain currents obtained from the DFT are then used to compute the far fields at all observation angles through the frequency-domain transformation [19]. To obtain necessary surface currents, the selected surface is a rectangular box that it's faces are 13 cells away from the outer boundaries, thus 3 cells away from the CPML interface and residing in the air gap region.

4.4. FDTD Results

The FDTD simulation of the implantable dual-band antenna is performed with 20,000 time steps, and s_{11} of the input port is

Calculated. The voltage between the ground plane and the probe is evaluated as a line integral of the electric field, while the current induced on the probe is obtained via a contour integral of the circumferential magnetic field around the probe. The calculated return loss is plotted in Fig. 6 and shows a good agreement with Fig. 4 (the published measurements data in [18]). The -10 dB bandwidths of the FDTD simulation in the MICS and ISM regions are 20.8% and 7%, respectively.

Furthermore, the directivity patterns are calculated in the xy, xz, and yz Plane cuts at 402 MHz and 2.4 GHz. These patterns are plotted in Figs. 7, 8, and 9, respectively. The results for 402 MHz are consistent with the gain characteristics of the MICS band implantable microstrip antennas in the literature [7].

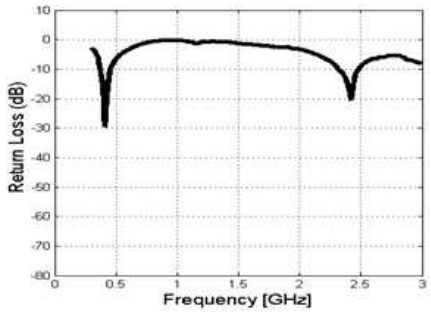

Figure 6. Return loss of the dual-band implantable antenna (FDTD result).

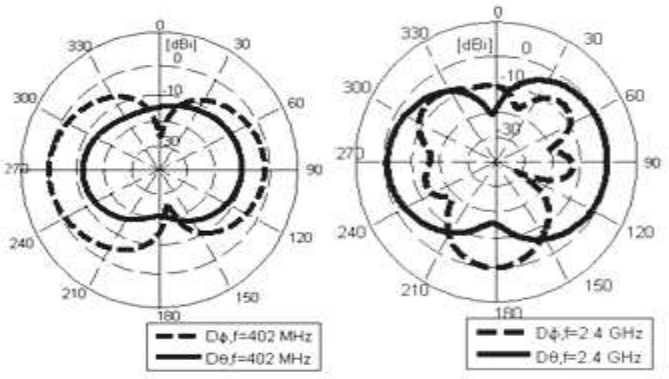

(a) 402 MHz (b) 2.4 MHz

Figure 7. Radiation patterns in the xy plane cut.

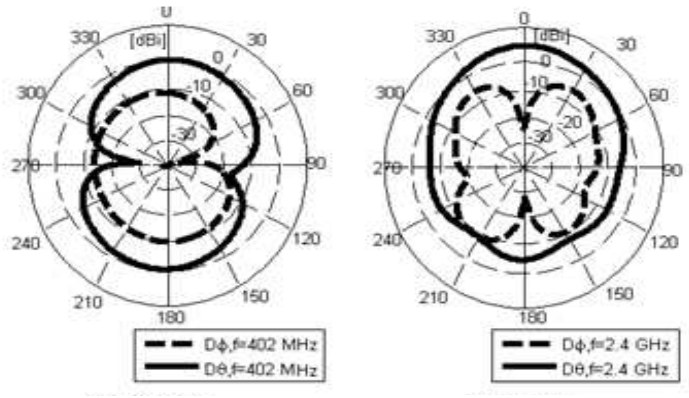

(a) 402 MHz (b) 2.4 MHz

Figure 8. Radiation patterns in the xz plane cut.

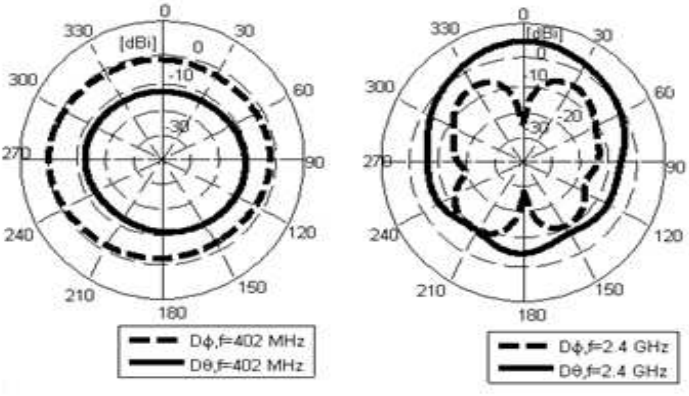

(a) 402 MHz (b) 2.4 MHz

Figure 9. Radiation patterns in the yz plane cut.

5. CONCLUSION

In this paper, we developed 2-pole Debye dispersion model of human dry skin at the MICS and ISM bands, and applied the model to analyses the resonance characteristics and far-zone electromagnetic fields of the dual-band implantable antenna for continuous glucose-monitoring applications. The return loss of the antenna was calculated using a simplified representation (one-layer structure) of the human

skin. The result shows a good agreement with the published measurements data. Furthermore, the directivity patterns were calculated in the xy, xz, and yz plane cuts at 402 MHz and 2.4 GHz.

We are currently working to calculate antenna radiation efficiency and the maximum delivered power for SAR considerations.

REFERENCES

1. Cavuoto, J., "Neural engineering's image problem," *IEEE Spectr.*, Vol. 41, No. 4, 32–37, Apr. 2004.
2. Furse, C. M., "Design of an antenna for pacemaker communication," *Microw. RF*, Vol. 39, No. 3, 73–76, Mar. 2000.
3. Schuster, J. and R. Luebbers, "An FDTD algorithm for transient propagation in biological tissue with a cole-cole dispersion relation," *IEEE AP/URSI Int. Symp. Dig.*, Vol. 4, 1988–1991, Jun. 1998.
4. Jacobsen, S. and P. R. Stauffer, "Multifrequency radiometric determination of temperature profiles in a lossy homogenous phantom using a dual-mode antenna with integral water bolus," *IEEE Trans. Microw. Theory Tech.*, Vol. 50, No. 7, 1737–1746, Jul. 2002.
5. Scanlon, W. G., N. E. Evans, and J. B. Burns, "FDTD analysis of closecoupled 418 MHz radiating devices for human biotelemetry," *Phys. Med. Biol.*, Vol. 44, 335–345, 1999.
6. Kim, J. and Y. Rahmat-Samii, "Implanted antennas inside a human body: Simulations, designs, and characterizations," *IEEE Trans. Microw. Theory Tech.*, Vol. 52, No. 8, 1934–1943, Aug. 2004.
7. Soontornpipit, P., C. Y. Furse, and Y. C. Chung, "Design of implantable microstrip antenna for communication with medical implants," *IEEE Trans. Microw. Theory Tech.*, Vol. 52, No. 8, 1944–1951, Aug. 2004.
8. Warty, R. and M. R. Tofighi, "Characterization of implantable antennas for intracranial pressure monitoring: Reflection by and transmission through a scalp phantom," *IEEE Trans. Microw. Theory Tech.*, Vol. 56, No. 10, Oct. 2008.
9. Kazuyuki, W., M. Takahashi, and K. Ito, "Performances of an implanted cavity slot antenna embedded in the human arm," *IEEE Trans. Antennas Propag.*, Vol. 57, No. 4, Apr. 2009.
10. Gabriel, C., S. Gabriel, and E. Corthout, "The dielectric properties of biological tissues: I. Literature survey," *Phys. Med. Biol.*, Vol. 41, 2231–2249, 1996.

11. Gabriel, S., R. W. Lau, and C. Gabriel, "The dielectric properties of biological tissues: II. Measurements in the frequency range 10 Hz to 20 GHz," *Phys. Med. Biol.*, Vol. 41, 2251–2269, 1996.
12. Gabriel, S., R. W. Lau, and C. Gabriel, "The dielectric properties of biological tissues: III. Parametric models for the dielectric spectrum of tissues," *Phys. Med. Biol.*, Vol. 41, 2271–2293, 1996.
13. Wuren, T., T. Takai, M. Fujii, and I. Sakagami, "Effective 2-Debye-pole FDTD model of electromagnetic interaction between whole human body and UWB radiation," *IEEE Microw. Wireless Compon. Lett.*, Vol. 17, No. 7, 483–485, Jul. 2007.
14. Lazebnik, M., M. Okoniewski, J. H. Booske, and S. C. Hagness, "Highly accurate Debye models for normal and malignant breast tissue dielectric properties at microwave frequencies," *IEEE Microw. Wireless Compon. Lett.*, Vol. 17, No. 12, Dec. 2007.
15. Fujii, M., R. Fujii, R. Yotsuki, T. Wuren, T. Takai, and I. Sakagami, "Exploration of whole human body and UWB radiation interaction by efficient and accurate two-Debye-pole tissue models," *IEEE Trans. Antennas Propag.*, Vol. 58, No. 2, Nov. 2010.
16. Guo, B., J. Li, and H. Zmuda, "A new FDTD formulation for wave propagation in biological media with cole-cole model," *IEEE Microw. Wireless Compon. Lett.*, Vol. 16, No. 12, Dec. 2006.
17. Mrozowski, M. and M. A. Stuchly, "Parametrization of media dispersive properties for FDTD," *IEEE Trans. Antennas Propag.*, Vol. 45, No. 9, 1438–1439, Sep. 1997.
18. Karacolak, T., A. Z. Hood, and E. Topsakal, "Design of a dual-band implantable antenna and development of skin mimicking gels for continuous glucose monitoring," *IEEE Trans. Microw. Theory Tech.*, Vol. 56, No. 4, 1001–1008, Apr. 2008.
19. Elsherbeni, A. and V. Demir, *The Finite-difference Time-domain Method for Electromagnetics with Matlab Simulations*, 484, 2009.
20. Mrozowski, M. and M. A. Stuchly, "Parameterization of media dispersive properties for FDTD," *IEEE Trans. Antennas Propag.*, Vol. 45, No. 9, 1438–1439, 1997.
21. Taflove, A. and S. C. Hagness, *Computational Electrodynamics: The Finite-difference Time-domain Method*, 3rd edition, Artech House, Boston, MA, 2005.
22. Abd El-Raouf, H. E., V. V. S. Prakash, J. Yeo, and R. Mittra, "FDTD simulation of a microstrip phased array with a coaxial feed," *IEE Proc. — Microw. Antennas Propag.*, Vol. 151, No. 3, Jun. 2004.

23. Hajiaboli, A. and M. Popovic, "FDTD subcell modeling of the ineer conductor of the coaxial feed: Accuracy and convergence analysis," *IEEE Trans. Magn.*, Vol. 43, No. 4, 1361–1364, Apr. 2007.
24. Riku, M. M. and A. K. Markku, "A stabilized resistive voltage source for FDTD thin-wire models," *IEEE Trans. Antennas Propag.*, Vol. 51, No. 7, Jul. 2003.
25. Taflove, A. and K. Umashankar, "Radar cross section of general three-dimensional structures," *IEEE Trans. Electromagn. Compat.*, Vol. 25, 433–440, 1983.
26. Huynh, M. C. and W. Stutzman, "Ground plane effects on planar inverted-f antenna (PIFA) performance," *Proc. Inst. Elect. Eng. Microw., Antennas Prop.*, Vol. 150, No. 4, 209–213, Aug. 2003.